Title

Algorithms for time-optimal control of CNC machines along curved tool paths

Journal

Robotics and Computer-Integrated Manufacturing, 21(1)

ISSN

0736-5845

Authors

Timar, Sebastian D
Farouki, R T
Smith, T S
et al.

Publication Date

2005-02-01

Peer reviewed

Algorithms for time–optimal control of CNC machines along curved tool paths

Sebastian D. Timar, Rida T. Farouki,
Tait S. Smith, and Casey L. Boyadjieff
Department of Mechanical and Aeronautical Engineering,
University of California, Davis, CA 95616.

Abstract

The problem of specifying the feedrate variation along a curved path, that yields minimum traversal time for a 3–axis CNC machine subject to constraints on the feasible acceleration along each axis, is addressed. In general, this time–optimal feedrate incurs "bang–bang control," i.e., maximum acceleration/deceleration is demanded of at least one axis throughout the motion. For a path defined by a polynomial parametric curve $\mathbf{r}(\xi)$, we show that the (square of the) time–optimal feedrate can be determined as a piecewise–rational function of the curve parameter ξ, with break–points corresponding to the roots of certain polynomial equations. Furthermore, this type of feedrate function is amenable to a real–time interpolator algorithm that drives the machine directly from the analytic curve description, eliminating the need for linear/circular G code approximations. The theoretical and computational aspects of such time–optimal feedrate functions are presented, together with experimental results from their implementation on a 3–axis mill driven by an open–architecture software controller.

Keywords: 3–axis machining; feedrate functions; acceleration constraints; time–optimal path traversal; bang–bang control; real–time interpolators.

e–mail addresses: sdtimar@ucdavis.edu, farouki@ucdavis.edu
tssmith@ucdavis.edu, clboyadjieff@ucdavis.edu

1 Introduction

In the context of CNC machining, the optimal specification of feedrate along curved tool paths has received little attention in the research literature. This is mainly due to the entrenched industry practice of approximating free–form curved paths by short linear/circular G code segments [1], which makes the realization of continuously–varying feedrates problematic. This reliance upon G codes is not necessitated by any limitations of the machine hardware, but rather by the interpolator algorithm in the control software, which interprets tool path and feedrate data in real time, so as to compute a "reference point" in each sampling interval ($\sim 10^{-3}$ sec.) of the servo system.

Recent years have witnessed increasing interest in real–time interpolators for analytic curves [3, 4, 13, 15, 18, 23, 25, 31, 33] which can provide variable–feedrate capability. Analytic curve descriptions provide complete information about path curvature, which is lost in G code approximations. The curvature information, together with continuous feedrate variations, offers the prospect for time–optimal traversal of free–form curved paths in a manner consistent with physical machine limitations (e.g., peak motor torques).

The Pythagorean–hodograph (PH) curves are especially well–suited [7, 8, 12, 30] to the formulation of real–time CNC interpolators, since they admit closed–form reduction of the interpolation integrals for feedrates dependent on time, arc length, or curvature. On the other hand, general (polynomial or rational) parametric curves require approximate methods based on truncated Taylor series expansions, whose development is increasingly cumbersome and error–prone beyond the quadratic or cubic term [13].

The problem of time–optimal traversal of a curved path, subject to bounds on the acceleration, has been extensively studied [2, 21, 24] in the context of robotic manipulator control, and has roots [27] in problems of rocket motion. The solutions to such control problems typically involve "bang–bang" inputs, in which the control variable jumps discontinuously between prescribed lower and upper bounds. These jumps occur at a finite number of locations, called *switching points*. Ordinarily, the control variable maintains its maximum or minimum value between successive switching points. In some circumstances, however, *critical segments* may also exist [21], along which the time–optimal solution incurs intermediate values of the control variable.

We are concerned in this paper with applying such methods to determine, for a CNC machine subject to prescribed acceleration bounds along each axis, the feedrate function that will minimize the traversal time along a polynomial

parametric curve $\mathbf{r}(\xi)$. For simplicity, we consider a 3–axis machine driven by independent motors on each axis, and we assume that inertial considerations dominate cutting forces, friction, etc. This problem is attractive because, as we shall see, the resulting differential equations are amenable to closed–form integration. Consequently, it is possible to determine switching points using polynomial root–finding methods, and to specify the time–optimal feedrate in terms of a piecewise–rational function of the curve parameter ξ. Furthermore, the latter admits an essentially exact real–time interpolator algorithm.

We shall proceed in this paper as follows. The basic principles governing time–optimal motion control problems along specified paths are summarized in §2. A step–by–step description of the general algorithm and an example are then provided in §3. In §4 we discuss the application of this methodology to the context of 3–axis CNC machines. Subsequent sections address specific aspects of the optimal feedrate solution in detail, including identification of break–points in the feedrate function, determined by the path geometry, in §5; construction of the "velocity limit curve" in §6; and the identification of "switching points" (transitions between minimal/maximal feed accelerations) and computation of the optimal feedrate function in §7. In §8 we develop a real–time interpolator algorithm that realizes the optimal feedrate, and in §9 experimental results from the implementation of this algorithm on a 3–axis mill with an open–architecture controller are presented. Finally, §10 summarizes our results and makes some concluding remarks.

2 Time–optimal control problems

Among the first practical problems addressed by the methods of time–optimal (or minimum time) control were those concerned with rocket trajectories [27]. A classical problem is that of specifying the rocket thrust that will transport a spacecraft at rest to some other position at rest in the least time. The solution involves "bang–bang" control — i.e., it requires that maximal forward thrust be applied up to the mid–point, then an instantaneous switching to maximal reverse thrust. Bang–bang control is characteristic of least–time execution of trajectories by physical systems of bounded motive force [14, 17].

More challenging time–optimal control problems have been studied in the field of motion planning for robotics. Algorithms to determine the minimum–time motion for a robot manipulator along a given path, under prescribed bounds on the acceleration for each joint, have been investigated since the

mid–80s. Among the key developments in this field are the papers by Bobrow, Dubowsky, and Gibson [2]; Pfeiffer and Johanni [19]; Shiller and co–workers [20, 21, 22]; Shin and McKay [24]; and Slotine and Yang [26, 32].

These methods employ phase–plane analysis and the fact that, in general, the time–optimal solution involves operating at the limit of one of the motive–force constraints at each instant during the traversal. Since the time–optimal control problem incurs a number of technical subtleties, and the above–cited references portray an evolutionary understanding of the complete solution, it seems appropriate to begin with a comprehensive review of the basic method, using a simplified notation suited to the particular application at hand. For an n degree–of–freedom manipulator, characterized by joint angles $\theta_1, \ldots, \theta_n$, the basic principles are as follows:

1. The path to be executed by the manipulator is specified by prescribing the joint coordinates as functions $\theta_1(s), \ldots, \theta_n(s)$ of a path parameter s [2, 19, 21, 24, 26]. Although s is often chosen to be arc length along the end–effector path, the analysis holds for any regular parameterization of the path [2, 24]. The n path variables $\theta_1, \ldots, \theta_n$ are thus reduced to a single continuous degree of freedom s.

2. The time derivative $v = \dot{s}$ of the arc length is the *feedrate* (speed) along the end–effector path — the analysis required to construct the optimal feedrate function $v(s)$ is conducted primarily in the (s, v) phase plane. The time derivative $a = \dot{v} = \ddot{s}$ of the feedrate is the *feed acceleration.* Since derivatives with respect to s may be transformed into derivatives with respect to time t through the chain rule

$$\frac{\mathrm{d}}{\mathrm{d}t} \;=\; \frac{\mathrm{d}s}{\mathrm{d}t}\frac{\mathrm{d}}{\mathrm{d}s} \;=\; v\,\frac{\mathrm{d}}{\mathrm{d}s}\,, \tag{1}$$

   the feed acceleration may also be written as

$$a \;=\; v\,\frac{\mathrm{d}v}{\mathrm{d}s}\,, \tag{2}$$

   — i.e., it is the product of v and the slope $\mathrm{d}v/\mathrm{d}s$ of a given trajectory at any point in the (s, v) phase plane. By means of (1) and (2), the derivatives of $\theta_1(s), \ldots, \theta_n(s)$ may be converted into time derivatives,

$$\dot{\theta}_k \;=\; v\,\frac{\mathrm{d}\theta_k}{\mathrm{d}s} \qquad \text{and} \qquad \ddot{\theta}_k \;=\; a\,\frac{\mathrm{d}\theta_k}{\mathrm{d}s} \;+\; v^2\frac{\mathrm{d}^2\theta_k}{\mathrm{d}s^2}\,,$$

for use in the equations of motion governing each joint, $k = 1, \ldots, n$. These equations, together with the associated torque constraints, give rise to a system of inequalities involving v, $a = v\,\mathrm{d}v/\mathrm{d}s$, and the known path functions $\theta_1(s), \ldots, \theta_n(s)$ and their derivatives.

3. For a prescribed path of total length S, the goal of the algorithm is to compute the feedrate function $v(s)$ that minimizes the traversal time

$$T = \int_0^S \frac{\mathrm{d}s}{v} \tag{3}$$

while satisfying, at each instant, the system of inequalities arising from the equations of motion and torque constraints for each joint. The first step of the algorithm is to identify a "feasible region" of the (s, v) phase plane, compatible with this system of inequalities.

4. If the torque exerted at each joint is subject to symmetric constraints, corresponding to a fixed negative lower bound and positive upper bound of equal magnitude, the resulting inequality at any position s is linear in v^2 and a, and may be interpreted as identifying an allowed region in the (v^2, a) plane. This region is the "strip" contained between a pair of parallel lines, symmetrically positioned relative to the origin. Taking all n joints into account, the overall allowed region is the intersection of n such strips, i.e., it is a parallelogram in the (v^2, a) plane with n pairs of parallel sides (see Figure 1). Of course, only the portion of this parallelogram in the right half of the plane ($v^2 \geq 0$) is of interest.

5. At each point of the specified path, the maximum feasible feedrate v_{lim} is identified by the right–most vertex of the parallelogram in the (v^2, a) plane. The variation $v_{\mathrm{lim}}(s)$ of this maximum speed with s is called the *velocity limit curve* (VLC) in the (s, v) phase plane — points below the VLC identify states that are compatible with all the torque bounds, but at least one of these bounds is violated for points above[1] the VLC.

[1]Early studies [2, 24] employed torque bounds dependent on the joint angles and angular velocities — for which the infeasible part of the (s, v) plane may include certain "islands" below the nominal VLC, as well as the region above it. Because of the difficulties incurred by such multiply–connected infeasible domains, subsequent studies [19, 21, 26] have focused on fixed torque bounds (which can always be chosen in a worst–case sense).

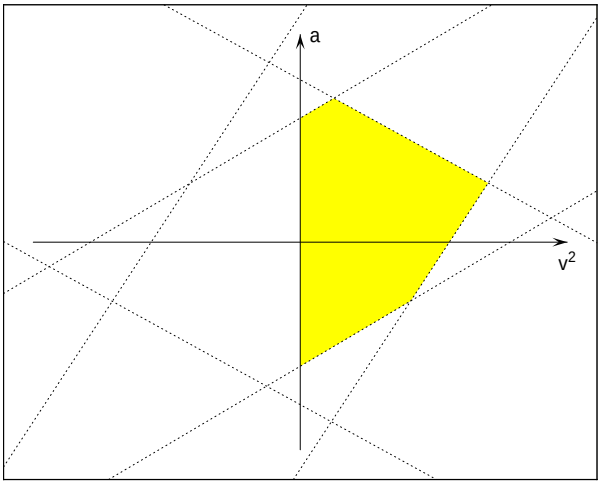

Figure 1: A set of (say) $n = 3$ pairs of linear symmetric constraints define the feasible region in the (v^2, a) plane as a $2n$–sided parallelogram at each point s along the prescribed path. Note that only the portion of this parallelogram lying in the right half of the (v^2, a) plane (the shaded region) is of interest.

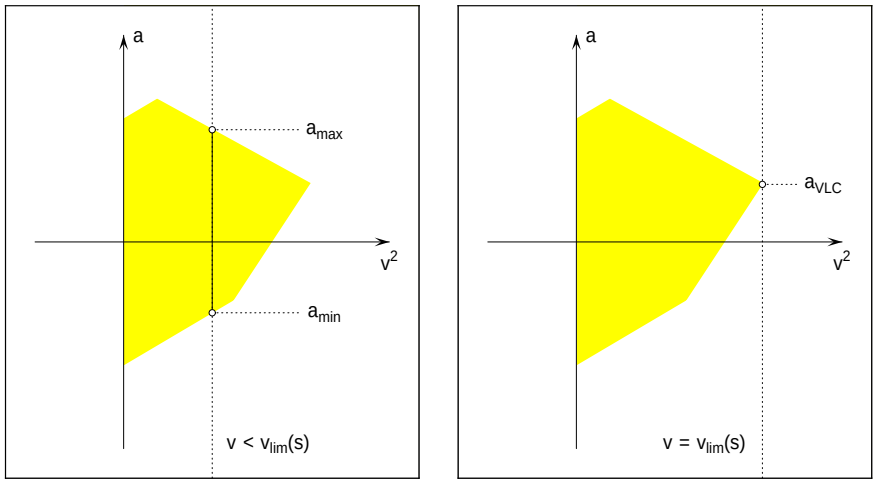

Figure 2: Left: for each state (s, v) with $v < v_{\rm lim}(s)$, a range of possible feed accelerations $a_{\rm min}(s, v) \leq a \leq a_{\rm max}(s, v)$ is defined by intersecting a vertical line with the parallelogram in the (v^2, a) plane. Right: when $v = v_{\rm lim}(s)$, the vertical line passes through the right–most vertex of the parallelogram, and the range of possible feed accelerations collapses to a single value, $a_{\rm VLC}(s)$.

6. For any state (s, v) below the VLC, $v < v_{\rm lim}(s)$, we can identify a range of possible feed accelerations

$$a_{\rm min}(s, v) \;\leq\; a \;\leq\; a_{\rm max}(s, v)$$

by intersecting a vertical line through v^2 with the parallelogram in the (v^2, a) plane [19, 21]: see Figure 2. At regular points $(s, v_{\rm lim}(s))$ on the VLC, this range collapses to a single possible value,

$$a_{\rm min}(s, v_{\rm lim}(s)) \;=\; a_{\rm max}(s, v_{\rm lim}(s))\,, \tag{4}$$

since a line through $v^2_{\rm lim}(s)$ intersects the parallelogram in a single point (its right–most vertex) rather than a range of values [2, 19, 21, 24, 26]: see Figure 2. The function specifying the unique value (4) of the feasible feed acceleration, on the VLC, is denoted[2] by $a_{\rm VLC}(s)$.

7. Depending upon how the vertical line intersects the parallelogram in the (v^2, a) plane, the bounds $a_{\rm min}(s, v)$ and $a_{\rm max}(s, v)$ on feed acceleration may be negative and positive, or both negative, or both positive (see Figure 2). Clearly, they must become both negative or both positive as v approaches $v_{\rm lim}(s)$, since they are coincident when $v = v_{\rm lim}(s)$.

8. Minimum–time path traversals generally involve a "bang–bang control" strategy, i.e., the feedrate $v(s)$ minimizing (3) is a piecewise–analytic function such that on alternate segments the upper and lower bounds on feed acceleration are continuously realized: $a = a_{\rm max}(s, v)$ or $a_{\rm min}(s, v)$. This means that one joint operates continuously at its torque limit on each segment. Each segment of the optimal feedrate $v(s)$ thus has an "active" constraint associated with it. Locations where a jump between $a_{\rm min}(s, v)$ and $a_{\rm max}(s, v)$ occur are called *switching points* [2, 21, 24, 26].

9. Early algorithms to compute time–optimal feedrates differed somewhat [2, 19, 24] but converged through later revisions [21, 22, 26]. The basic principles governing all these methods are consistent[3] with each other:

    1. Integrate forwards (i.e., increasing s) from $(0, 0)$ in the (s, v) phase plane with maximum feed acceleration, $\dot{v} = a_{\rm max}(s, v)$.

[2]Note that the feasible feed acceleration $a_{\rm VLC}$ on the VLC does *not*, in general, equal the feed acceleration $v_{\rm lim}{\rm d}v_{\rm lim}/{\rm d}s$ that corresponds to using $v_{\rm lim}(s)$ as the feedrate.

[3]For simplicity, we assume boundary conditions $v = 0$ at $s = 0$ and $s = S$ — positive initial/final feedrates can also be used.

2. Integrate backwards (decreasing s) from $(S, 0)$ in the (s, v) phase plane with minimum feed acceleration, $\dot{v} = a_{\min}(s, v)$.
3. If the integration trajectories meet at a point below the VLC, their intersection (s, v) is the sole switching point. If they meet the VLC before intersecting, however, intermediate switching points will be required, some of which will lie on the VLC.

10. Three types of switching points may occur on the VLC: *tangency points*, *critical points*, and *discontinuity points* [26].

    (a) *Tangency points* occur where the (unique) feed acceleration of an integration trajectory is equal to the feed acceleration that results from using $v_{\lim}(s)$ as the feedrate function, i.e., we have

    $$a_{\mathrm{VLC}}(s) \;=\; v_{\lim}(s)\,\frac{\mathrm{d}v_{\lim}}{\mathrm{d}s}(s)\,.$$

    This means that, at tangency points, the slope of an integration trajectory in the (s, v) phase plane coincides with the slope of the VLC [19, 21, 24, 26]. Segments of the VLC are called trajectory *sources* or *sinks*, according to whether the integration trajectories at each point on them have slopes smaller than or greater than the slope of the VLC [19, 21, 26]. Hence, tangency points generally separate[4] trajectory source and sink segments on the VLC [21].

    (b) *Critical points* correspond to slope discontinuities of the VLC — symptomatic of a change in the identity of the constraints defining $v_{\lim}(s)$. Unlike smooth VLC points, where integration trajectories possess a unique feed acceleration $a_{\mathrm{VLC}}(s)$, a range of possible feed accelerations exists at a critical point [19, 21, 26]. Critical points are also called "zero inertia" points, since they identify locations s where the coefficient of a in any one of the constraints vanishes, and hence that constraint is purely on v^2 [26]: the parallelogram in the (v^2, a) plane has a pair of vertical parallel sides (see Figure 3).

    Exceptionally, the "zero inertia" condition may be sustained for an interval $s \in [\,a, b\,]$ rather than just an isolated point, and the corresponding portion of the VLC is called a *critical segment* [21].

[4] However, this separation property may not hold in exceptional cases, involving higher–order contact of integration trajectories with the VLC.

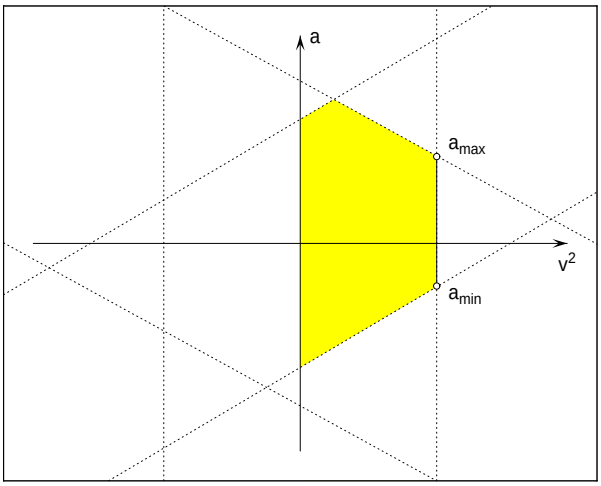

Figure 3: At a critical point on the VLC, one pair of constraints in the (v^2, a) plane is described by vertical lines — i.e., these constraints depend only on v^2 and not on a. Thus, instead of a unique value $a_{\mathrm{VLC}}(s)$ of the feed acceleration at such points, there is a range of possible values $a_{\min} \leq a \leq a_{\max}$ instead.

Critical points on the VLC admit distinct lower and upper bounds, $a_{\min}(s, v_{\lim}(s))$ and $a_{\max}(s, v_{\lim}(s))$, on the feed acceleration, rather than a unique value $a_{\mathrm{VLC}}(s)$. Comparing these bounds with the left and right limits of the feed acceleration that corresponds to using $v_{\lim}(s)$ as the feedrate, the conditions[5]

$$a_{\min}(s, v_{\lim}(s)) \; > \; v_{\lim}(s) \, \frac{\mathrm{d}v_{\lim}}{\mathrm{d}s}(s^-) \tag{5}$$

and

$$a_{\max}(s, v_{\lim}(s)) \; < \; v_{\lim}(s) \, \frac{\mathrm{d}v_{\lim}}{\mathrm{d}s}(s^+) \tag{6}$$

must be satisfied for the critical point to be a potential switching point. If either condition is not satisfied we have a *singular* critical point [22], and if either is not satisfied on an interval in s we have a *singular critical segment* of the VLC [22].

Because of the incompatibility of the feed acceleration bounds at a singular critical point with the feed acceleration corresponding to

[5]When $\mathrm{d}v_{\lim}/\mathrm{d}s$ is discontinuous at any point s, we indicate its distinct left and right limits at that point by using the symbols s^- and s^+ to denote its argument.

$v_{\lim}(s)$, it is impossible for integration trajectories to arrive at or depart from such points, and hence they cannot serve as switching points. In [22] it is suggested that a trajectory should "slide" along the VLC in the neighborhood of a singular critical point. Recall, however, that the unique feasible feed acceleration a_{VLC} at regular VLC points differs from the value $v_{\lim}\mathrm{d}v_{\lim}/\mathrm{d}s$ incurred by using $v_{\lim}(s)$ as the feedrate. Hence, a trajectory coincident with $v_{\lim}(s)$ over any finite extent must be in violation of at least one constraint (except in the case of a critical segment).

(c) *Discontinuity points* arise if the path functions $\theta_1(s), \ldots, \theta_n(s)$ are not C^2 continuous everywhere. If they are only C^0 at some points, the feedrate v must vanish at such points, since an instantaneous change of direction with $v \neq 0$ implies an infinite acceleration. The optimal feedrate may be thus computed by subdividing the path at each C^0 point, and solving independent optimal feedrate problems on the sub–intervals they delineate [26]. If the path functions are only C^1 at certain points (corresponding to discontinuities in path curvature), the VLC is discontinuous in value at these points. The *smaller* of the two VLC values, $v_{\lim}(s^-)$ and $v_{\lim}(s^+)$, about such discontinuities identifies a potential switching point [26], and the appropriate feed acceleration at that point is the value associated with the smaller of these two VLC values.

11. The optimal feedrate function incorporates isolated points of the VLC only where the tangency conditions are met, or where (non–singular) critical points occur. Furthermore, it incorporates finite segments of the VLC if the tangency conditions are satisfied at every point, or along critical segments (intervals along which the effective inertia is zero and the acceleration bounds are compatible with the VLC).

3 Time–optimal feedrate algorithm

Based on the principles enumerated in §2, the algorithm for computing the time–optimal feedrate function [21] may be summarized as follows (again, we assume that $v = 0$ at $s = 0$ and $s = S$ — non–zero initial/final feedrates may be substituted if desired):

0. Pre–process: compute the velocity limit curve $v_{\lim}(s)$, and the ordered sequence of all (potential) switching points, and their types, on it.

1. Integrate $\dot{v} = a_{\max}(s, v)$ forward from the initial condition $(s, v) = (0, 0)$ and $\dot{v} = a_{\min}(s, v)$ backward from the final condition $(s, v) = (S, 0)$ — denote these integration trajectories[6] by $v_1(s)$ and $v_N(s)$, respectively, where N is the number of segments (to be determined) comprising the time–optimal feedrate function $v(s)$.

2. If the two integration trajectories intersect at a point beneath the VLC, i.e., $v_1(s_1) = v_N(s_1) < v_{\lim}(s_1)$ for some $s_1 \in (0, S)$, then s_1 is the only switching point, and the time–optimal feedrate function $v(s)$ comprises just $N = 2$ segments:

$$v(s) = \begin{cases} v_1(s) & \text{for } s \in [\, 0, s_1 \,] \,, \\ v_2(s) & \text{for } s \in [\, s_1, S \,] \,. \end{cases}$$

3. If the two initial trajectories do not intersect below the VLC, they must cross the VLC at (distinct) "left" and "right" points, $(s_l, v_{\lim}(s_l))$ and $(s_r, v_{\lim}(s_r))$. From $(s_l, v_{\lim}(s_l))$ search forwards along the VLC for the first occurrence of a switching (tangent, critical, or discontinuity) point on the VLC, and denote this switching point by $(s_2, v_{\lim}(s_2))$.

4. Generate an $a_{\min}$ trajectory $v_2(s)$ arriving at $(s_2, v_{\lim}(s_2))$ by integrating $\dot{v} = a_{\min}(s, v)$ backwards until it intersects the initial $a_{\max}$ trajectory $v_1(s)$ at a point $(s_1, v_1(s_1))$, where $0 < s_1 < s_2$. The value s_1 identifies the first switching point of the optimal feedrate $v(s)$, whose first two segments now comprise $v_1(s)$ for $s \in [\, 0, s_1 \,]$ and $v_2(s)$ for $s \in [\, s_1, s_2 \,]$.

5. Now generate an $a_{\max}$ trajectory $v_3(s)$ departing from $(s_2, v_{\lim}(s_2))$ by integrating $\dot{v} = a_{\max}(s, v)$ forwards until it intersects: (i) the final $a_{\min}$ trajectory $v_N(s)$ — go to step **6**; or (ii) the VLC — go to step **7**.

6. In case (i), let the point where the $a_{\max}$ trajectory $v_3(s)$ intersects the final $a_{\min}$ trajectory $v_N(s)$ be s_3. Then $N = 4$, and $v(s)$ is completed by augmenting the current state with $v_3(s)$ for $s \in [\, s_2, s_3 \,]$ and $v_4(s)$ for

[6] Although earlier authors [19, 21, 22] call them "maximum acceleration trajectories" and "maximum deceleration trajectories" we refer to the loci in the (s, v) plane obtained by integrating $\dot{v} = a_{\max}(s, v)$ and $\dot{v} = a_{\min}(s, v)$ as "$a_{\max}$ trajectories" and "$a_{\min}$ trajectories" since it is not necessarily true that $a > 0$ and $a < 0$ at each point of the former and latter.

$s \in [\, s_3, S\,]$. Hence, $v(s)$ comprises four segments delineated by three switching points s_1, s_2, s_3 (s_2 identifies a switching point on the VLC, while s_1, s_3 identify switching points below the VLC). **END**

7. In case (ii), search forwards on the VLC from where the $a_{\max}$ trajectory $v_3(s)$ intersects the VLC for the first occurrence of a switching point on the VLC, which we label $(s_4, v_{\lim}(s_4))$.

8. Generate an $a_{\min}$ trajectory $v_4(s)$ arriving at $(s_4, v_{\lim}(s_4))$ by integrating $\dot{v} = a_{\min}(s, v)$backwards to the point s_3 where it crosses the incoming $a_{\max}$ trajectory $v_3(s)$ — this point s_3 identifies the third switching point of the optimal feedrate function $v(s)$.

9. Now generate an $a_{\max}$ trajectory $v_5(s)$ departing from $(s_4, v_{\lim}(s_4))$ by integrating $\dot{v} = a_{\max}(s, v)$ forwards until it intersects: (i) the final $a_{\min}$ trajectory $v_N(s)$; or (ii) the VLC.

10. In case (i), $N = 6$, and $v(s)$ may be completed in a manner analogous to step **6**. In case (ii), we need to find the first occurrence of a switching point on the VLC beyond its intersection with $v_5(s)$, and then construct an arriving $a_{\min}$ trajectory and departing $a_{\max}$ trajectory from this switching point, in a manner analogous to steps **7**–**9**.

11. We iterate this basic process of finding the next VLC switching point (beyond the intersection of the current $a_{\max}$ trajectory with the VLC), and computing incoming $a_{\min}$ and outgoing $a_{\max}$ trajectories from this switching point, until the outgoing $a_{\max}$ trajectory intersects the final $a_{\min}$ trajectory $v_N(s)$ instead of the VLC. The optimal feedrate then comprises an even total number N of segments, delineated by $N - 1$ switching points. Furthermore, switching points on the VLC alternate with switching points below the VLC (which correspond to intersections of $a_{\max}$ and $a_{\min}$ trajectories).

At tangency switching points, a unique feed acceleration $a_{\min}(s, v_{\lim}(s)) = a_{\max}(s, v_{\lim}(s)) = a_{\mathrm{VLC}}(s)$ exists for trajectories arriving at or departing from such points. At critical switching points $a_{\min}(s, v_{\lim}(s)) < a_{\max}(s, v_{\lim}(s))$ and a range of feed accelerations is possible. Finally, at singular critical points one of these two bounds is incompatible with the VLC, since the inequalities (5) and (6) are not satisfied, so they are disqualified as switching points.

Note that the components $v_k(s)$ of the optimal feedrate function are not necessarily analytic on the respective intervals $s \in [\, s_{k-1}, s_k \,]$ for $k = 1, \ldots, N$ (where $s_0 = 0$ and $s_N = S$), since within these intervals the path geometry may incur a change of the axis corresponding to the "active" constraint. If this occurs at a point $s_* \in (s_{k-1}, s_k)$, then $v_k(s)$ has different forms on the two intervals $[\, s_{k-1}, s_* \,]$ and $[\, s_*, s_k \,]$ even though s_* is not identified by the algorithm as a switching point.

Our goal in this paper is to adapt the optimal feedrate algorithm to the problem of 3–axis machining, under the assumption that inertial forces incurred by the accelerations of the machine axes are dominant, and cutting forces, friction, etc. are comparatively small (as in the context of high–speed machining of complex shapes). Although the optimal feedrate algorithm for CNC machines with independent Cartesian axes is in some respects simpler than for multi–joint robot manipulators, it admits derivation of a closed–form expression (rather than a numerical approximation) for the optimal feedrate function. Moreover, real–time CNC interpolators can be developed to obtain realization of this function by simple replacement of the existing interpolator module in the overall control software architecture.

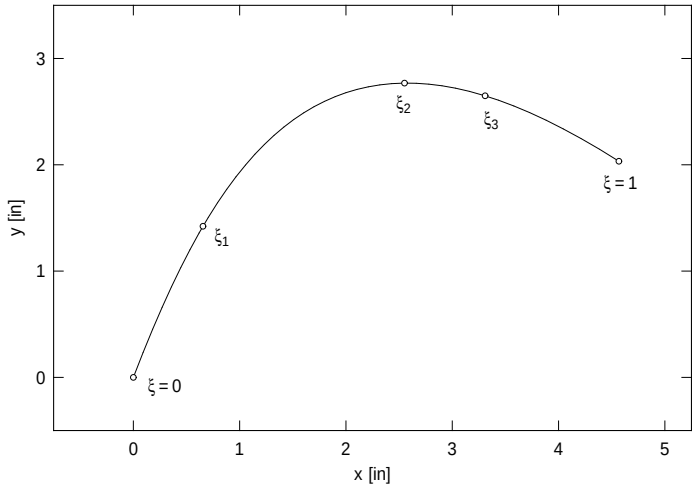

Figure 4: Planar path $\mathbf{r}(\xi)$ for the determination of a time–optimal feedrate. The intervals $[\, 0, \xi_1 \,]$ and $[\, \xi_2, \xi_3 \,]$ are $a_{\max}$ segments, while $[\, \xi_1, \xi_2 \,]$ and $[\, \xi_3, 1 \,]$ are $a_{\min}$ segments (see Figure 5). Switching point ξ_2 corresponds to a critical point on the VLC, while the switching points ξ_1 and ξ_3 identify intersections of $a_{\max}$ and $a_{\min}$ trajectories below the VLC.

In the context of driving a CNC machine along a polynomial parametric curve $\mathbf{r}(\xi)$, it is more convenient[7] to use the curve parameter ξ rather than arc length s. Complete details on each step of the algorithm, in this context, are developed in §4 below. However, it is instructive to first present a simple example, to help elucidate the method. The path geometry shown in Figure 4 is a plane polynomial curve, $\mathbf{r}(\xi)$ for $\xi \in [\,0, 1\,]$. In Figure 5 we illustrate the construction of the time–optimal feedrate $v(\xi)$ in the (ξ, v) phase plane.[8] The VLC, $v_{\lim}(\xi)$, is the piecewise–analytic locus bounding the shaded region of infeasible states that violate at least one of the acceleration constraints.

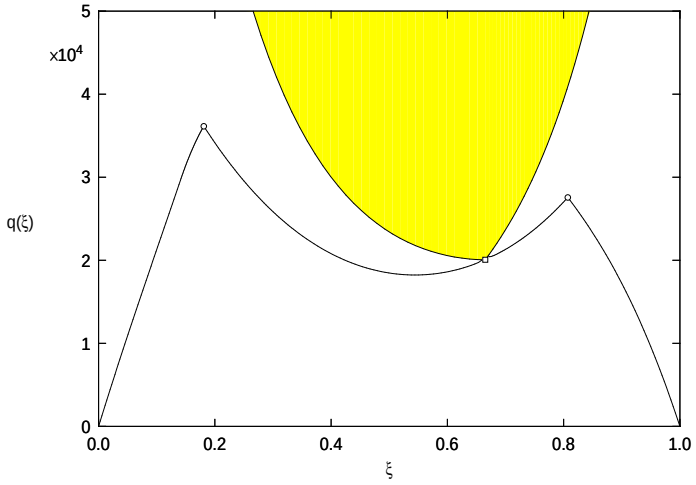

Figure 5: Construction of time–optimal feedrate for the curve in Figure 4. The shaded region is the set of infeasible states, bounded by the VLC, $v_{\lim}(\xi)$. The time–optimal feedrate has four segments, delineated by switching points: namely, $a_{\max}$ segments on $[\,0, \xi_1\,]$ and $[\,\xi_2, \xi_3\,]$, and $a_{\min}$ segments on $[\,\xi_1, \xi_2\,]$ and $[\,\xi_3, 1\,]$. As explained in §4 below, it is more convenient to employ the square of the feedrate, $q = v^2$, in the construction.

Integrating $\dot{v} = a_{\max}(\xi, v)$ forward from $(\xi, v) = (0, 0)$ to obtain $v_1(\xi)$, we observe that this $a_{\max}$ trajectory intersects the VLC at some point ξ_l. Also, integrating $\dot{v} = a_{\min}(\xi, v)$ backward from $(\xi, v) = (1, 0)$ to obtain $v_N(\xi)$, we

[7] It is impossible [11] to parameterize any curve, other than a straight line, by rational functions of the arc length — in general, numerical procedures are required to determine corresponding values of the curve parameter ξ and arc length s.

[8] The figure actually shows the square $q = v^2$ of the feedrate, which is computationally a more convenient quantity.

see that this $a_{\min}$ trajectory intersects the VLC at some point ξ_r. The fact that the initial and final trajectories intersect the VLC before they cross each other indicates that intermediate switching points on the VLC are required. Searching forward along the VLC from the intersection of $v_1(\xi)$ and $v_{\lim}(\xi)$ we encounter a critical point, labelled ξ_2.

Now since the conditions (5)–(6) are satisfied, the critical point ξ_2 is not singular, and it is possible to integrate an $a_{\min}$ trajectory $v_2(\xi)$ backward from $(\xi_2, v_{\lim}(\xi_2))$. This is observed to intersect the initial $a_{\max}$ trajectory at the point labelled ξ_1. Hence, $v_1(\xi)$ for $\xi \in [\,0, \xi_1\,]$ and $v_2(\xi)$ for $\xi \in [\,\xi_1, \xi_2\,]$ define the first two segments of the time–optimal feedrate. Similarly, we can integrate an $a_{\max}$ trajectory $v_3(\xi)$ forward from $(\xi_2, v_{\lim}(\xi_2))$ and this is found to intersect $v_N(\xi)$ at the point labelled ξ_3. We therefore deduce that $N = 4$, and the time–optimal feedrate is completed by adding the segments $v_3(\xi)$ for $\xi \in [\,\xi_2, \xi_3\,]$, and $v_4(\xi)$ for $\xi \in [\,\xi_3, 1\,]$.

4 Application to 3–axis machining

Consider a path described by a degree–n Bézier curve

$$\mathbf{r}(\xi) \;=\; \sum_{k=0}^{n} \mathbf{p}_k \binom{n}{k} (1-\xi)^{n-k} \xi^k \,, \quad \xi \in [\,0, 1\,] \tag{7}$$

with control points $\mathbf{p}_k = (x_k, y_k, z_k)$, $k = 0, \ldots, n$ [6]. If s denotes arc length measured along the curve, we define the *parametric speed* by

$$\sigma(\xi) \;=\; |\mathbf{r}'(\xi)| \;=\; \frac{\mathrm{d}s}{\mathrm{d}\xi} \,.$$

The unit tangent and (principal) normal vectors and the curvature of (7) are defined by

$$\mathbf{t} \;=\; \frac{\mathbf{r}'}{\sigma} \,, \qquad \mathbf{n} \;=\; \frac{\mathbf{r}' \times \mathbf{r}''}{|\mathbf{r}' \times \mathbf{r}''|} \times \mathbf{t} \,, \qquad \kappa \;=\; \frac{|\mathbf{r}' \times \mathbf{r}''|}{\sigma^3} \tag{8}$$

and, conversely, with $\sigma' = (\mathbf{r}' \cdot \mathbf{r}'')/\sigma$ we may write

$$\mathbf{r}' \;=\; \sigma\, \mathbf{t} \,, \qquad \mathbf{r}'' \;=\; \sigma'\, \mathbf{t} \;+\; \sigma^2 \kappa\, \mathbf{n} \,. \tag{9}$$

Now suppose we traverse the curve with feedrate (speed) specified by the function $v(\xi)$. Since derivatives with respect to time t and the parameter ξ

— which we denote by dots and primes, respectively — are related by

$$\frac{\mathrm{d}}{\mathrm{d}t} = \frac{\mathrm{d}s}{\mathrm{d}t}\frac{\mathrm{d}\xi}{\mathrm{d}s}\frac{\mathrm{d}}{\mathrm{d}\xi} = \frac{v}{\sigma}\frac{\mathrm{d}}{\mathrm{d}\xi},$$

the velocity and acceleration vectors at each point are given by

$$\mathbf{v} = \dot{\mathbf{r}} = v\,\mathbf{t}, \qquad \mathbf{a} = \ddot{\mathbf{r}} = \dot{v}\,\mathbf{t} + \kappa v^2\,\mathbf{n}. \tag{10}$$

The *tangential* component $\dot{v}\,\mathbf{t}$ of $\mathbf{a}$ vanishes if $v =$ constant, while the *normal* (*centripetal*) component $\kappa v^2\,\mathbf{n}$ vanishes if $\kappa = 0$. The time derivative of the feedrate (the *feed acceleration*) can be expressed in terms of ξ as $\dot{v} = vv'/\sigma$.

We wish to minimize the traversal time along $\mathbf{r}(\xi)$, starting and ending at rest, subject to prescribed limits on the acceleration along each machine axis.[9] This requirement can be phrased as the following optimization problem:

$$\min_{v(\xi)} T = \int_0^1 \frac{\sigma}{v}\,\mathrm{d}\xi \tag{11}$$

such that

$$|a_x(\xi)| \le A_x\,, \quad |a_y(\xi)| \le A_y\,, \quad |a_z(\xi)| \le A_z \quad \text{for } \xi \in [\,0,1\,]$$

where (a_x, a_y, a_z) denote the Cartesian components of $\mathbf{a}$, and (A_x, A_y, A_z) are corresponding bounds on the acceleration magnitude along each axis.

4.1 Extremal trajectories

Using (8), (10), and the relations $\sigma\sigma' = \mathbf{r}'\cdot\mathbf{r}''$, $\dot{v} = vv'/\sigma$, we may write

$$\mathbf{a} = \frac{vv'}{\sigma^2}\,\mathbf{r}' + \frac{v^2}{\sigma^3}\,(\sigma\mathbf{r}'' - \sigma'\mathbf{r}'),$$

and hence the components of $\mathbf{a}$ are given by

$$\begin{aligned} a_x &= \frac{vv'}{\sigma^2}\,x' + \frac{v^2}{\sigma^3}\,(\sigma x'' - \sigma' x'),\\ a_y &= \frac{vv'}{\sigma^2}\,y' + \frac{v^2}{\sigma^3}\,(\sigma y'' - \sigma' y'),\\ a_z &= \frac{vv'}{\sigma^2}\,z' + \frac{v^2}{\sigma^3}\,(\sigma z'' - \sigma' z'), \end{aligned}$$

[9] These limits are determined by the inertia of the axes, and the torque capacity of the drive motors — they are especially important in *high–speed machining* [16, 28, 29].

where $x(\xi)$, $y(\xi)$, $z(\xi)$ are the components of $\mathbf{r}(\xi)$. It is convenient to work with the *square* of the feedrate, $q = v^2$, in terms of which we have

$$\begin{aligned} a_x &= \frac{q'}{2\sigma^2}\,x' + \frac{q}{\sigma^3}\,(\sigma x'' - \sigma' x')\,, \\ a_y &= \frac{q'}{2\sigma^2}\,y' + \frac{q}{\sigma^3}\,(\sigma y'' - \sigma' y')\,, \\ a_z &= \frac{q'}{2\sigma^2}\,z' + \frac{q}{\sigma^3}\,(\sigma z'' - \sigma' z')\,. \end{aligned} \tag{12}$$

During an $a_{\max}$ or $a_{\min}$ phase, one component of the acceleration is plus or minus the corresponding limit. For example, if x is the limiting axis, we have

$$\frac{q'}{2\sigma^2}\,x' + \frac{q}{\sigma^3}\,(\sigma x'' - \sigma' x') = \pm A_x\,, \tag{13}$$

which may be re–arranged to obtain

$$q' + 2\left(\frac{x''}{x'} - \frac{\sigma'}{\sigma}\right) q = \pm\frac{2A_x\sigma^2}{x'}\,. \tag{14}$$

This linear differential equation for q may be solved by first multiplying both sides by the integrating factor $(x'/\sigma)^2$ to obtain

$$\frac{\mathrm{d}}{\mathrm{d}\xi}\left(\frac{x'}{\sigma}\right)^2 q = \pm 2A_x x'\,,$$

and hence we deduce the closed–form solution

$$q = \left(\frac{\sigma}{x'}\right)^2 (C \pm 2A_x x)\,, \tag{15}$$

where the integration constant C is determined by specifying a known point (ξ_*, q_*) on the trajectory: $C = (x'(\xi_*)/\sigma(\xi_*))^2\, q(\xi_*) \mp 2A_x x(\xi_*)$.

However, if $x'(\xi_*) = 0$, special care is required because the denominator of expression (15) vanishes. Since the feedrate must be finite, the numerator of (15) must also vanish at ξ_* if q is to have a finite limit value as $\xi \to \xi_*$. This determines the constant as $C = \mp 2A_x x(\xi_*)$. Furthermore, writing $f = \sigma^2(C \pm 2A_x x)$ and $g = x'^2$, we have $f(\xi_*) = f'(\xi_*) = 0$ and $g(\xi_*) = g'(\xi_*) = 0$, so L'Hopital's rule gives

$$\lim_{\xi\to\xi_*} q(\xi) = \frac{f''(\xi_*)}{g''(\xi_*)} = \pm A_x\,\frac{\sigma^2(\xi_*)}{x''(\xi_*)}\,.$$

Note that this is consistent with the value given by (13) when $x' = 0$.

For a curve of degree n, expression (15) specifies q as a rational function in ξ with numerator of degree $3n-2$ and denominator of degree $2n-2$. By a proper choice of the integration constant C, this function is non–singular even at points where $x' = 0$. If a feedrate segment starts or ends at a point with $x' = 0$, and this segment is re–parameterized to the interval $\xi \in [\,0,1\,]$, the polynomials $f(\xi)$ and $g(\xi)$ have $\xi = 0$ or $\xi = 1$ as a common double root. To avoid numerical problems evaluating (15) near such points, it is advisable to cancel the common factor ξ^2 or $(1-\xi)^2$ from $f(\xi)$ and $g(\xi)$, yielding a reduction in degree by 2. This is easily accomplished by noting that if

$$p(\xi) \;=\; \sum_{k=0}^{m} c_k \binom{m}{k} (1-\xi)^{m-k} \xi^k$$

is a Bernstein–form polynomial with $c_0 = c_1 = 0$, we can write it as

$$p(\xi) \;=\; \xi^2 \sum_{k=0}^{m-2} \tilde{c}_k \binom{m-2}{k} (1-\xi)^{m-2-k} \xi^k \,,$$

where

$$\tilde{c}_k \;=\; \frac{\binom{m}{k+2}}{\binom{m-2}{k}}\, c_{k+2} \qquad \text{for } \; k = 0, \ldots, m-2\,.$$

Similarly, if $c_{m-1} = c_m = 0$, we can write

$$p(\xi) \;=\; (1-\xi)^2 \sum_{k=0}^{m-2} \tilde{c}_k \binom{m-2}{k} (1-\xi)^{m-2-k} \xi^k \,,$$

where

$$\tilde{c}_k \;=\; \frac{\binom{m}{k}}{\binom{m-2}{k}}\, c_k \qquad \text{for } \; k = 0, \ldots, m-2\,.$$

Analogous results hold when the limiting axis is y or z, rather than x.

Now from equation (14) we observe that the x–motion imposes the limits[10]

$$2\left(\frac{\sigma'}{\sigma} - \frac{x''}{x'}\right) q \;-\; \frac{2A_x\sigma^2}{x'} \;\le\; q' \;\le\; 2\left(\frac{\sigma'}{\sigma} - \frac{x''}{x'}\right) q \;+\; \frac{2A_x\sigma^2}{x'} \qquad (16)$$

[10] We assume $x' > 0$ at the given ξ value; otherwise these limits would be swapped.

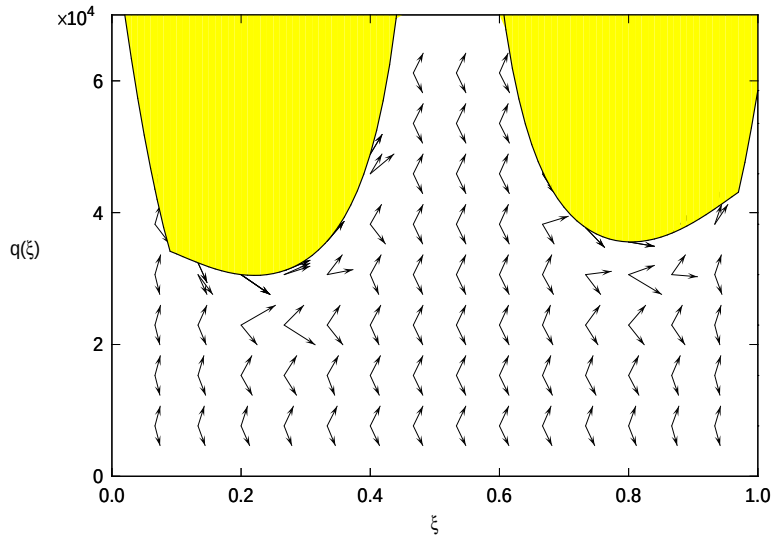

Figure 6: Range of possible slopes q' for trajectories in the (ξ, q) phase plane, at sample points below the velocity limit curve, $q_{\rm lim}(\xi) = v^2_{\rm lim}(\xi)$. The VLC has two critical points (slope discontinuities), and a singularity near $\xi = 0.5$.

on the slope $q' = {\rm d}q/{\rm d}\xi$ of any trajectory through a given point of the (ξ, q) phase plane. Similar limits result from the y– and z–motions, and hence the range of possible q' values

$$q' \in [\, q'_{\rm min}, q'_{\rm max} \,] \tag{17}$$

for each (ξ, q) is the intersection of the ranges imposed by each of the three axes (or, equivalently, by intersecting a vertical line through $q = v^2$ with the parallelogram of possible (v^2, a) values). Note that the slope q' of a trajectory in the (ξ, q) plane is a measure of the feed acceleration a, since $q' = 2\sigma a$. The range (17) of possible q' values collapses to a single value as q approaches $q_{\rm lim}$ (except at ξ values identifying critical points of the VLC).

Figure 6 shows the variation of the q' range, at a sampling of points below the VLC, for a representative example. It is evident that, upon approaching the VLC, the q' range collapses to a single value. Note also that, because of sudden changes in the constraints determining $q'_{\rm min}$ and $q'_{\rm max}$, these limits are continuous, but not differentiable, functions of location in the (ξ, q) plane.

5 Break–points of optimal feedrate

We now discuss how the parallelogram of possible (v^2, a) values may be used to identify certain break–points of the optimal feedrate function, and how these break–points are related to the path geometry. Moreover, the identities of the constraints that determine $a_{\min}$ and $a_{\max}$ at each point, and of the "active" constraint on each interval between break–points, is analyzed.

5.1 Set of possible $(v^2, \dot{v})$ values

For brevity, we consider henceforth a plane curve $\mathbf{r}(\xi) = (x(\xi), y(\xi))$ as tool path, the extension to spatial paths being relatively straightforward but more tedious to fully enumerate. We write q and v^2 interchangeably for the square of the feedrate, and $\dot{v}$ and a for the feed acceleration. Assuming that inertial forces dominate cutting forces and friction, and the maximum motor torque for each axis is independent of its position, speed, and direction, the bounds on the x and y acceleration components yield the inequalities

$$\begin{aligned} -A_x \;\le\; t_x(\xi)\,\dot{v} + \kappa(\xi) n_x(\xi)\,v^2 \;\le\; +A_x\,, \\ -A_y \;\le\; t_y(\xi)\,\dot{v} + \kappa(\xi) n_y(\xi)\,v^2 \;\le\; +A_y\,, \end{aligned} \tag{18}$$

where A_x and A_y are the acceleration bounds for the x and y axes. Here, the dependence of the tangent $\mathbf{t} = (t_x, t_y)$ and normal $\mathbf{n} = (n_x, n_y)$ components and the curvature κ on the curve parameter ξ are explicitly indicated.

At each ξ, the inequalities (18) define the interior of a parallelogram as the set of possible $(v^2, \dot{v})$ values. The pairs of parallel sides of this parallelogram correspond to the $\pm$ instances of expressions (18) for the axis acceleration bounds, using the equality signs. As ξ increases, this parallelogram varies in size, shape, and orientation. The four vertices of the parallelogram may be identified by taking equality signs in (18) and solving

$$t_x\,\dot{v} + \kappa n_x\,v^2 \;=\; \alpha_x A_x\,, \quad t_y\,\dot{v} + \kappa n_y\,v^2 \;=\; \alpha_y A_y\,, \tag{19}$$

where $\alpha_x = \pm 1$ and $\alpha_y = \pm 1$, as simultaneous linear equations to obtain

$$v^2 \;=\; \frac{A\sigma^2}{x'y'' - x''y'}\,(\alpha_y x' - \alpha_x y')\,, \quad \dot{v} \;=\; \frac{A}{\sigma}\,(\alpha_x x' + \alpha_y y')\,. \tag{20}$$

Here we use $\mathbf{t} = (x', y')/\sigma$, $\mathbf{n} = (-y', x')/\sigma$, and $\kappa = (x'y'' - x''y')/\sigma^3$ for the tangent, normal, and curvature of $\mathbf{r}(\xi) = (x(\xi), y(\xi))$, and further assume that the x and y acceleration bounds are equal: $A_x = A_y = A$ (say).

Now only the portion of the parallelogram in the right half ($v^2 \geq 0$) of the $(v^2, \dot{v})$ plane is relevant, and expressions (20) yield two vertices in the left half of the $(v^2, \dot{v})$ plane and two in the right half, as we exercise the four possible sign combinations $(\alpha_x, \alpha_y) = (\pm 1, \pm 1)$. Knowing the two vertices on the right allows us to identify which three among the four constraints defined by (19) with $(\alpha_x, \alpha_y) = (\pm 1, \pm 1)$ bound the portion of the parallelogram in the right half of the $(v^2, \dot{v})$ plane. Each of these may serve as the "active" constraint during an $a_{\min}$ or $a_{\max}$ integration, and as ξ increases from 0 to 1 the identity of the active constraint changes at certain points.

Thus, the problem of specifying the time–optimal feedrate $v(\xi)$ on a curve $\mathbf{r}(\xi)$ involves determining a partition of the $\xi \in [\,0, 1\,]$ interval such that, on each sub–interval, the known identity of the "active" constraint is constant. Moreover, according to whether it corresponds to an $a_{\min}$ or $a_{\max}$ phase — or, exceptionally, a portion of the VLC — the analytic form of $v(\xi)$ on each of these sub–intervals must be determined.

5.2 Vertices of the $(v^2, \dot{v})$ parallelogram

The four sign combinations $(\alpha_x, \alpha_y) = (\pm 1, \pm 1)$ in (20) each identify a unique vertex of the parallelogram of possible $(v^2, \dot{v})$ values. Furthermore, one may verify from (20) that the four vertices always lie in distinct quadrants of the $(v^2, \dot{v})$ plane. At certain values of ξ that correspond to special properties of the path geometry, however, the vertices identified by particular sign choices (α_x, α_y) may switch between the lower and upper, or left and right, halves of the $(v^2, \dot{v})$ plane. Another important case is characterized by configurations in which the parallelogram has vertical sides, since this may incur a transition in the identity of the "lower" and "upper" constraints defining $a_{\min}$ and $a_{\max}$.

Such points must be identified *a priori*, since they entail changes in the analytic form of the time–optimal feedrate (although they are not switching points in the sense described in §2). These break–points for the time–optimal feedrate function correspond to inflections, turning points, and points where the x and y components of the curve tangent have equal magnitude (which we call "equi–orientation" points). To identify subsets of $\xi \in [\,0, 1\,]$ over which the identities of the constraints defining the upper and lower boundaries of the set of possible $(v^2, \dot{v})$ are invariant, we examine each of them in turn.

Inflections

From the expression $\kappa = (x'y'' - x''y')/\sigma^3$ for the curvature of a plane curve, we see that at an inflection ($\kappa = 0 \neq \kappa'$) the denominator of v^2 vanishes in the expressions (20) for the vertices of the parallelogram of possible $(v^2, \dot{v})$ values. Thus, on passing through a parameter value ξ that corresponds to an inflection, the pairs of vertices in the left and right half–planes recede[11] to $-\infty$ and $+\infty$, and then re–appear in the right and left half–planes, respectively. The identities of the constraints passing through the pairs of vertices in the left and right half–planes are therefore swapped on traversing an inflection. The parameter values of inflections can be easily found as (odd multiplicity) roots of $x'(\xi)y''(\xi) - x'(\xi)y''(\xi) = 0$ on $\xi \in [\,0, 1\,]$.

Turning points

At turning points we have $x' = 0$ or $y' = 0$ — i.e., the curve tangent makes an angle $k\pi/2$, $k = 0, 1, 2, 3$ with the positive x direction. At such points, the coordinates (20) of the parallelogram vertices indicate that they can be grouped into pairs with the same value of v^2, and hence two of the constraints correspond to vertical lines. Such configurations define a transitional state of the set of possible $(v^2, \dot{v})$ values — the portion of the parallelogram in the right half–plane changes from having a "lower" boundary defined by two constraints and an "upper" boundary defined by one constraint, to a "lower" boundary defined by one constraint and an "upper" boundary defined by two constraints, or vice–versa (Figure 7). Hence, the identities of the constraints defining $a_{\min}$ and $a_{\max}$ may change as we pass through a turning point. The (odd multiplicity) roots of the equations $x'(\xi) = 0$ and $y'(\xi) = 0$ on $\xi \in [\,0, 1\,]$ identify the parameter values of turning points.

Equi–orientation points

From (20) we observe that a parallelogram vertex crosses from the left to the right half–plane, or vice–versa, when the condition

$$\alpha_y x' \;=\; \alpha_x y'$$

is satisfied for a particular choice of signs (α_x, α_y). If ξ is a parameter value such that $|x'(\xi)| = |y'(\xi)|$, this condition must be satisfied for one of the four

[11] At inflections, the centripetal component $\kappa v^2\,\mathbf{n}$ of the acceleration vanishes, leaving only the tangential component $\dot{v}\,\mathbf{t}$ — hence the constraints involve only $\dot{v}$ at inflections.

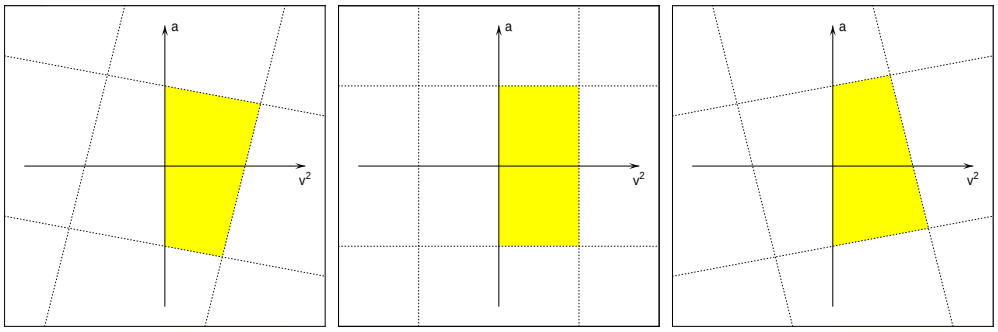

Figure 7: Behavior of set of possible (v^2, a) values at a turning point. Left: before the turning point, two constraints define the lower boundary, and one defines the upper boundary. Center: at the turning point, the two pairs of constraints are horizontal and vertical. Right: after the turning point, one constraint defines the lower boundary, and two define the upper boundary.

combinations $(\alpha_x, \alpha_y) = (\pm 1, \pm 1)$. We call points satisfying $|x'(\xi)| = |y'(\xi)|$ "equi–orientation points" since the curve tangent makes equal (non–oriented) angles with the x and y axes (i.e., it makes an oriented angle of $(2k+1)\pi/4$, $k = 0, 1, 2, 3$ with the positive x direction). The parameter values incurring this condition are the roots of the equation $x'^2(\xi) - y'^2(\xi) = 0$ on $\xi \in [\,0, 1\,]$.

Similarly, we note from (20) that when the condition

$$\alpha_x x' \;=\; -\,\alpha_y y'$$

is satisfied for a particular (α_x, α_y) then a parallelogram vertex crosses from the lower to the upper half–plane, or vice–versa. Again, if $|x'(\xi)| = |y'(\xi)|$, this condition must be satisfied for one of the cases $(\alpha_x, \alpha_y) = (\pm 1, \pm 1)$. The circumstances for vertices to cross between the lower and upper halves of the $(v^2, \dot{v})$ plane are thus identical to those for crossing between the left and right halves — they also arise at equi–orientation points.

This coincidence is a consequence of the fact that, for simplicity, we have assumed acceleration bounds satisfying $A_x = A_y$ $(= A,$ say). Thus, at equi–orientation points, the parallelogram of possible $(v^2, \dot{v})$ values assumes the shape of a diamond with two vertices on the v^2 axis, and two vertices on the $\dot{v}$ axis — a single constraint applies within each quadrant.

If we partition the curve parameter domain $\xi \in [\,0, 1\,]$ by the values that identify inflections, turning points, and equi–orientation points, we obtain a

set of sub–domains over which the identities of the constraints defining the upper and lower boundaries of the set of possible $(v^2, \dot{v})$ values do not change. This set comprises the right–hand portion of the parallelogram defined by (18) with $A_x = A_y = A$ (the upper boundary is defined by two constraints and the lower boundary by one constraint, or vice–versa). Over each sub–domain, the unique identity[12] of the constraints defining these upper and lower boundaries can be determined *a priori*. Thus, given a current position ξ and feedrate v, it is possible to integrate an $a_{\min}$ or $a_{\max}$ trajectory backward or forward within such sub–domains, to obtain an analytic component of the time–optimal feedrate $v(\xi)$. In fact, as we shall see in §7, this integration admits a closed–form expression for $v(\xi)$.

In addition to inflections, turning points, and equi–orientation points, a fourth type of possible break–point in the time–optimal feedrate, which we call a *transition* point, must be accounted for. Unlike the former three types of break–point, transition points depend not only on the local curve geometry, but also on the current feedrate v. Hence, they cannot be identified *a priori* by analysis of the curve alone — they must be determined during the process of integration to obtain the time–optimal feedrate.

Transition points

Within any sub-domain of $\xi \in [\,0, 1\,]$ delineated by inflections, turning points, and equi–orientation points, the set of possible $(v^2, \dot{v})$ values is bounded by $v^2 = 0$ and three of the four constraints defined by (19) with $(\alpha_x, \alpha_y) = (\pm 1, \pm 1)$. The lower boundary of this set is defined by two constraints and the upper boundary is defined by a single constraint, or vice–versa. For the boundary defined by two constraints, the vertex at which the two constraints meet corresponds to the instance of (20) with $(\alpha_x, \alpha_y) = (\pm 1, \pm 1)$ that yields the smaller of the two positive v^2 values. If, for example, the lower boundary is defined by two constraints meeting at a point (v_*^2, a_*) for curve parameter value ξ_*, then the identity of the "active" constraint changes as we integrate an $a_{\min}$ trajectory passing through the phase–plane point (ξ_*, v_*) — a change in the analytic form of the time–optimal feedrate $v(\xi)$ will be necessary at this point. The same principles apply if the upper boundary is defined by two constraints and we are integrating an $a_{\max}$ trajectory.

[12] The identity of a constraint is specified by the axis (x or y) to which it applies, and the corresponding sign α_x or α_y in (19).

Once all the break–points have been found, the sub–domains of $\xi \in [\,0,1\,]$ they define may each be labelled with the corresponding "active" constraint, and a specification of whether they correspond to an $a_{\min}$ or $a_{\max}$ segment.

6 Velocity limit curve

At each point along the curve $\mathbf{r}(\xi)$, the maximum possible feedrate $v_{\lim}(\xi)$ is identified by the right–most vertex of the parallelogram of possible states in the $(v^2, \dot{v})$ plane [19, 21]. This vertex is identified by a unique combination of signs (α_x, α_y) in the solution (20) of equations (19). Care must be exercised in constructing the velocity limit curve $v_{\lim}(\xi)$, since it exhibits certain generic pathological features. At turning points, the parallelogram of possible $(v^2, \dot{v})$ values has a right–most vertical side instead of a right–most vertex, and at inflections $v_{\lim}(\xi) \to \infty$, since the curvature vanishes: the acceleration has a tangential, but no centripetal, component. Both points incur changes in the identity — the (α_x, α_y) combination — of the vertex that defines $v_{\lim}(\xi)$.

6.1 VLC critical points

As the constraints that define the set of possible $(v^2, \dot{v})$ values vary with ξ, changes in the sign combination (α_x, α_y) that identifies the right–most of the parallelogram vertices (20) occur at curve *turning points*, where

$$t_x \,=\, 0 \qquad \text{or} \qquad t_y \,=\, 0\,. \tag{21}$$

At such points, the pair of constraints (19) associated with one machine axis (x or y) becomes independent of $\dot{v}$ — i.e., they are represented by vertical lines in the $(v^2, \dot{v})$ plane (simultaneously, the constraints for the other axis become horizontal lines, since $t_x = 0 \Rightarrow n_y = 0$ and $t_y = 0 \Rightarrow n_x = 0$). This condition marks a sudden change in the identity of the vertex that defines $v_{\lim}$ — at such points $v_{\lim}$ is continuous in value, but not in its derivative. Thus, turning points are VLC *critical points* — tangent–discontinuous points where the slope $v'_{\lim}$ has different left and right limits [21]. For the first condition in (21), the constraints become

$$\dot{v} \,=\, \pm A\,, \qquad v^2 \,=\, \pm\frac{A\sigma^2}{x''}\,,$$

while for the second condition in (21) they become

$$\dot{v} \;=\; \pm A\,, \qquad v^2 \;=\; \pm\frac{A\sigma^2}{y''}\,.$$

Thus, one constraint bounds only the feed acceleration, and the other bounds only the feedrate. Turning points, where the machine motion swaps between axes, are therefore not only critical points of the VLC, but also "zero inertia" points [21] of the system — one axis incurs no limit on the feed acceleration.

6.2 VLC singularities

At inflections of $\mathbf{r}(\xi)$, where $\kappa = 0$, the constraints (19) become independent of v. Approaching an inflection, the right–most vertex of the parallelogram of possible $(v^2, \dot{v})$ values recedes to infinity as all four constraints become horizontal lines. Consequently the VLC exhibits a singularity, $v_{\text{lim}} \to \infty$, at inflections. Since the curvature changes sign on passing through an inflection, there is a corresponding change in the combination of signs (α_x, α_y) in (20) identifying the parallelogram vertex that defines v_{lim}.

7 Optimal feedrate computation

The time–optimal feedrate consists of a piecewise–analytic function, defined on a partition of the $\xi \in [\,0, 1\,]$ curve domain. The break–points are related to the path geometry, as described in §5, or are switching points on or below the VLC. The "active" constraint on each sub–domain of the partition is known by analysis of the parallelogram of possible $(v^2, \dot{v})$ values (see §5), and the time–optimal feedrate algorithm, sketched in §3, determines whether each sub–domain corresponds to an a_{min} or a_{max} integration trajectory.

The square of the feedrate on each subdomain is then given by a rational expression of the form (15). Exceptionally, when the VLC exhibits critical segments, the feedrate on some sub–domains may be defined by $q_{\text{lim}}(\xi)$ rather than integration of an a_{min} or a_{max} trajectory.

In computing the optimal feedrate, switching points are locations that incur an abrupt change between a_{min} and a_{max} trajectory integrations [2, 24, 19, 26, 21]. For C^2 curves, the possible types of switching point are:

(a) intersections of a_{min} and a_{max} trajectories below the VLC;

(b) points where $a_{\min}$ or $a_{\max}$ trajectories are tangent to the VLC;

(c) (non–singular) VLC critical points.

7.1 Type (a) switching points

Intersections of $a_{\min}$ and $a_{\max}$ feedrate trajectories always occur as the first and last switching points in cases with multiple switchings, and are the only switching point in cases where the entire optimal feedrate lies below the VLC.

7.2 Type (b) switching points

The function $q_{\lim}(\xi) = v^2_{\lim}(\xi)$ has a unique slope $q'_{\lim}$ at each smooth point of the VLC, which may be compared to the range of admissible slopes (17) for that point. If $q'_{\lim} < q'_{\min}$, every trajectory at that point vanishes into the infeasible region above the VLC: such points are trajectory *sinks*. Conversely, if $q'_{\lim} > q'_{\max}$, every trajectory at that point emerges into the feasible region below the VLC: such points are trajectory *sources*. Transitions from VLC sink to source points, or vice–versa, are characterized by a coincidence of $q'_{\lim}$ with $q'_{\min}$ or $q'_{\max}$ — i.e., tangency of an $a_{\min}$ or $a_{\max}$ trajectory to the VLC [24, 19, 26, 21]. Such (potential) switching points are identified as follows.

The VLC is defined by the expression for v^2 in (20), with appropriate choices for (α_x, α_y). Defining the quantities

$$f \;=\; \alpha_y x' - \alpha_x y' \qquad \text{and} \qquad g \;=\; x'y'' - x''y' \,,$$

we may write

$$q_{\lim} \;=\; v^2_{\lim} \;=\; \frac{A\sigma^2 f}{g} \,.$$

Differentiating this expression, the slope of the VLC in the (ξ, q) plane may be expressed as

$$q'_{\lim} \;=\; A \left[\frac{2\sigma\sigma' f}{g} + \frac{\sigma^2 f'}{g} - \frac{\sigma^2 f g'}{g^2} \right] . \tag{22}$$

On the other hand, the only possible feed acceleration $a_{\rm VLC}$ along the VLC is the unique value (except at critical points) defined by the right–most vertex of the parallelogram of possible (v^2, a) values. It is given by the expression

for $\dot{v}$ in (20), with the same combination of signs (α_x, α_y) used in $q_{\lim} = v_{\lim}^2$. Using $q' = 2\sigma\dot{v}$, we define $q'_{\rm VLC} = 2\sigma a_{\rm VLC}$ and substitute from (20) to obtain

$$q'_{\rm VLC} \;=\; 2A(\alpha_x x' + \alpha_y y')\,,$$

which we write as

$$q'_{\rm VLC} \;=\; 2Ah\,, \tag{23}$$

where

$$h \;=\; \alpha_x x' + \alpha_y y'\,.$$

Tangency switching points are characterized by the condition $q'_{\rm VLC} = q'_{\lim}$. Equating (22) to (23) and simplifying, these switching points correspond to (simple) roots of the polynomial equation

$$2hg^2 - 2\sigma\sigma' fg + \sigma^2(fg' - f'g) \;=\; 0\,. \tag{24}$$

These roots identify changes from sink to source segments, or vice–versa, on the VLC. Note that this polynomial must be constructed individually for each analytic segment of the VLC, defined by a particular (α_x, α_y) combination, allowing the roots within the domain of that segment to be computed.

Exceptionally, the multiple roots (if any) of equation (24) identify higher–order contact of an $a_{\min}$ or $a_{\max}$ trajectory with the VLC. Depending on their multiplicity, they may or may not identify potential switching points.

7.3 Type (c) switching points

At critical points (slope discontinuities) of the VLC, a range of possible feed accelerations, rather than a unique value, exists. In order for a critical point to serve as a switching point, the lower and upper bounds of this range must be compatible with the distinct left and right slopes of the VLC — i.e., the critical point must be non–singular. Singular critical points, which do not satisfy the conditions (5) and (6), cannot serve as switching points, since it is impossible for either an $a_{\min}$ trajectory to arrive at, or an $a_{\max}$ trajectory to depart from, such points. In [22] it is suggested that integration trajectories should be allowed to "slide" along the VLC in the vicinity of singular critical points. However, since the unique feasible feed acceleration $a_{\rm VLC}$ at regular VLC points differs from the value $v_{\lim}\mathrm{d}v_{\lim}/\mathrm{d}s$ incurred by using $v_{\lim}$ as the feedrate, this incurs violation of at leat one acceleration constraint.

7.4 Treatment of transition points

If the upper or lower boundary of the set of possible $(v^2, \dot{v})$ values is defined by two constraints, a change in the feedrate expression will occur when we are integrating an $a_{\max}$ or $a_{\min}$ trajectory, respectively, and the current state (ξ, v) is such that v coincides with the value for the parallelogram vertex defined by these two constraints. This value is given by the expression for v^2 in (20) using the combination of signs (α_x, α_y) that yields the smaller of the two positive v^2 values (the larger positive v^2 value defines the VLC).

If the current active constraint corresponds to the x axis, the parameter value ξ that identifies a transition vertex may be determined by equating the expressions for $q = v^2$ in (15) and (20) to obtain the polynomial equation

$$(C + 2\alpha_x A x)(x'y'' - x'y'') - A x'^2(\alpha_y x' - \alpha_x y') \;=\; 0\,,$$

where α_x, α_y are unique to the vertex under consideration. The smallest of the roots larger than the last break–point of the feedrate function is taken as the transition point, and a new feedrate expression (corresponding to the new active constraint) is required on the next ξ interval.

8 Real–time interpolator

Prior to invoking the real–time CNC interpolator for time–optimal feedrates, the curve is first subdivided such that along each segment the (square of the) feedrate is described by a single rational function. In particular, knowing the active constraint for each segment, the feedrate along it is given by the square root of an expression of the form (15) or (20), according to whether it corresponds to an $a_{\min}$ or $a_{\max}$ segment, or a portion of the VLC.

Knowing the curve geometry and desired feedrate variation, the function of the real–time interpolator is to compute, within each sampling interval Δt of the digital controller, a "reference point" indicating the commanded machine position. If ξ_k is the reference–point parameter value at time $k\Delta t$, the equation that determines this value is

$$k\Delta t \;=\; \int_0^{\xi_k} \frac{\sigma}{v}\,\mathrm{d}\xi\,, \tag{25}$$

since $\mathrm{d}\xi/\mathrm{d}t = (\mathrm{d}s/\mathrm{d}t)(\mathrm{d}\xi/\mathrm{d}s) = v/\sigma$. For the case where v corresponds to an $a_{\min}$ or $a_{\max}$ segment (with, say, x as the limiting axis), substituting the

square root of (15) into (25) gives

$$k\Delta t \;=\; \int_0^{\xi_k} \frac{|x'|}{\sqrt{C + 2\alpha_x A x}}\,\mathrm{d}\xi\,,$$

which admits closed–form integration to obtain

$$k\Delta t \;=\; \frac{\sqrt{C + 2\alpha_x A\, x(\xi_k)}}{A} \;+\; K\,, \tag{26}$$

the integration constant K being chosen such that $t = 0$ when $\xi = 0$ (note that each curve segment is re–parameterized so as to have domain $\xi \in [\,0, 1\,]$). The parameter value ξ_k may be found from (26) by an iterative (e.g., Newton–Raphson) method [12]. Since ξ is a monotone–increasing function of t, this equation has only one real root: starting from ξ_{k-1}, a few iterations typically suffice for convergence to ξ_k within machine precision.

Along a critical segment, where the feedrate is defined by the VLC, the interpolation integral (25) does not admit a simple closed–form reduction, and we must employ a Taylor series expansion [13] to estimate ξ_k:

$$\xi_k \;=\; \xi_{k-1} \;+\; \frac{\mathrm{d}\xi}{\mathrm{d}t}\,\Delta t \;+\; \frac{\mathrm{d}^2\xi}{\mathrm{d}t^2}\,(\Delta t)^2 \;+\; \cdots\,. \tag{27}$$

Here, time derivatives are transformed into derivatives with respect to ξ using

$$\frac{\mathrm{d}}{\mathrm{d}t} \;=\; \frac{v}{\sigma}\,\frac{\mathrm{d}}{\mathrm{d}\xi}\,,$$

which gives

$$\frac{\mathrm{d}\xi}{\mathrm{d}t} \;=\; \frac{v}{\sigma}\,, \quad \frac{\mathrm{d}^2\xi}{\mathrm{d}t^2} \;=\; \frac{v}{\sigma}\,\frac{\mathrm{d}}{\mathrm{d}\xi}\left(\frac{v}{\sigma}\right) \;=\; \frac{v(\sigma v' - \sigma' v)}{\sigma^3}\,, \quad \cdots \quad \text{etc.}$$

where primes denote ξ derivatives, and v is given by the square root of (20) when x is the limiting axis. These expressions are to be evaluated at ξ_{k-1} for use in (27).

9 Experimental results

The fact that the velocity limit curve and $a_{\min}$, $a_{\max}$ trajectories are known (piecewise) rational loci in the (ξ, q) phase plane allows us to compute the

time–optimal feedrate using only polynomial root–finding algorithms, which can be robustly implemented using the numerically–stable Bernstein form [9, 10] on $\xi \in [\,0, 1\,]$. Computation of the optimal feedrate is performed by an off–line program, that receives a curve and acceleration bounds as input, and outputs a piecewise–rational function for the (square of the) feedrate.

We describe here experimental results for two representative test curves, one without switching points on the VLC, and the other with switching points on the VLC — shown, respectively, in Figures 8 and 9. Acceleration bounds $A_x = A_y = 10^4$ in/min^2 were specified for both curves. The experiments were performed on a precision 3–axis CNC mill, driven by an open–architecture software controller, that permits incorporation of the real–time interpolator algorithms described above in §8. The controller has a sampling frequency of 1024 Hz. By computing first and second differences of the real–time position data, recorded by encoders on the machine axes during each run, the velocity and acceleration performance can be assessed *a posteriori*.

Figure 8 shows the time–optimal squared feedrate function $q(\xi)$ for the first test curve in the (ξ, q) phase plane — in this instance, $q(\xi)$ is a piecewise–rational function with just one switching point below the VLC delineating two segments: an $a_{\max}$ segment up to the switching point, and an $a_{\min}$ segment thereafter. No switching points on the VLC are required in this case.

Similarly, Figure 9 shows the time–optimal squared feedrate function for the second test curve. In this case, $q(\xi)$ is a piecewise–rational function with five switching points delineating switches between $a_{\max}$ and $a_{\min}$ phases. Two of the switching points lie on the velocity limit curve in this case.

Figures 10–12 and Figures 13–15 show velocity and acceleration data from runs on the first and second test curves, respectively. In Figures 10 and 13 we illustrate separately the x and y components of the velocity for each curve, obtained by differencing of measured positional data. Figures 11 and 14 show the magnitude of the feedrate — note that, in these plots, the independent variable is the elapsed time t, rather than the curve parameter ξ.

Figures 12 and 15 illustrate the x and y components of the acceleration for each curve, obtained by second differencing of measured position data — the "noise" is a consequence of the differencing operation. It is apparent that the optimal feedrate derived by the algorithm of §4 does indeed correspond to a "bang–bang" control strategy — i.e., the acceleration magnitude on either the x or the y axis attains the prescribed bounds of $\pm 10^4$ in/min^2 throughout the motion. Furthermore, the time–optimal feedrate functions are accurately realized by the real–time interpolator algorithms described in §8.

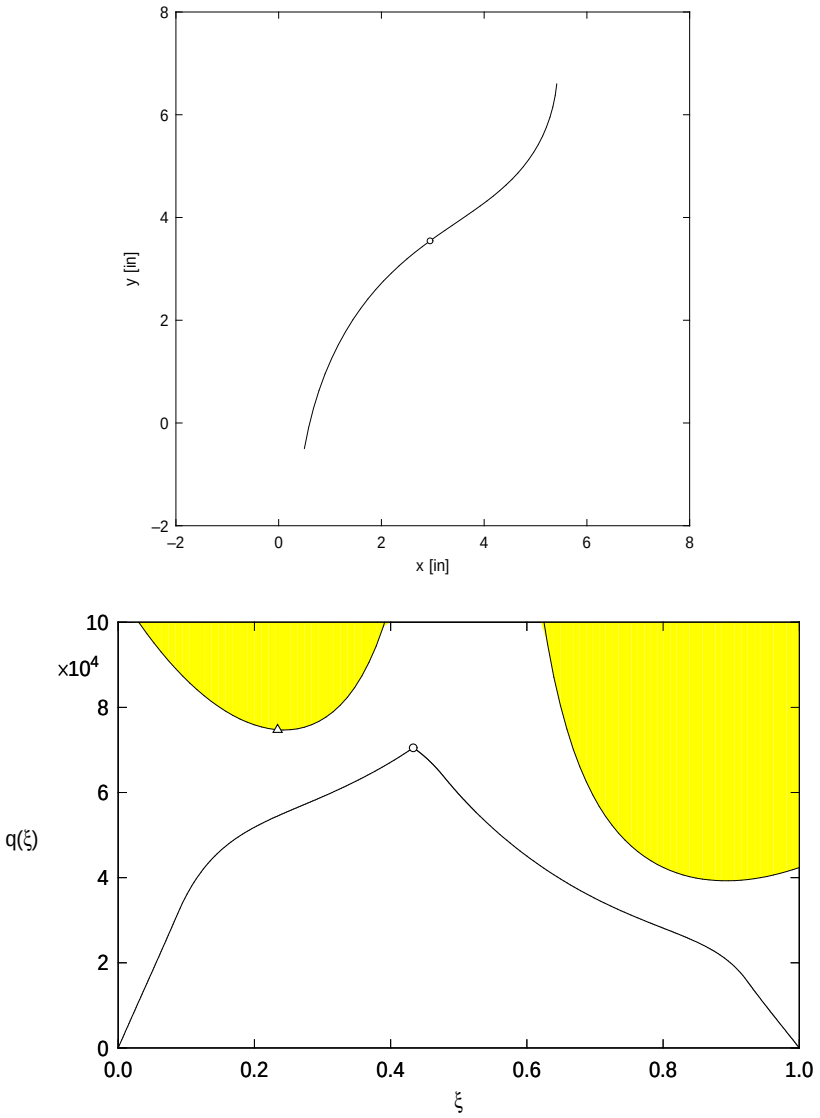

Figure 8: Test curve $\mathbf{r}(\xi)$ (upper) and square of time–optimal feedrate $q(\xi)$ (lower) with switching points indicated. In this case, the only switching point lies below the velocity limit curve, and $q(\xi)$ is a piecewise–rational function.

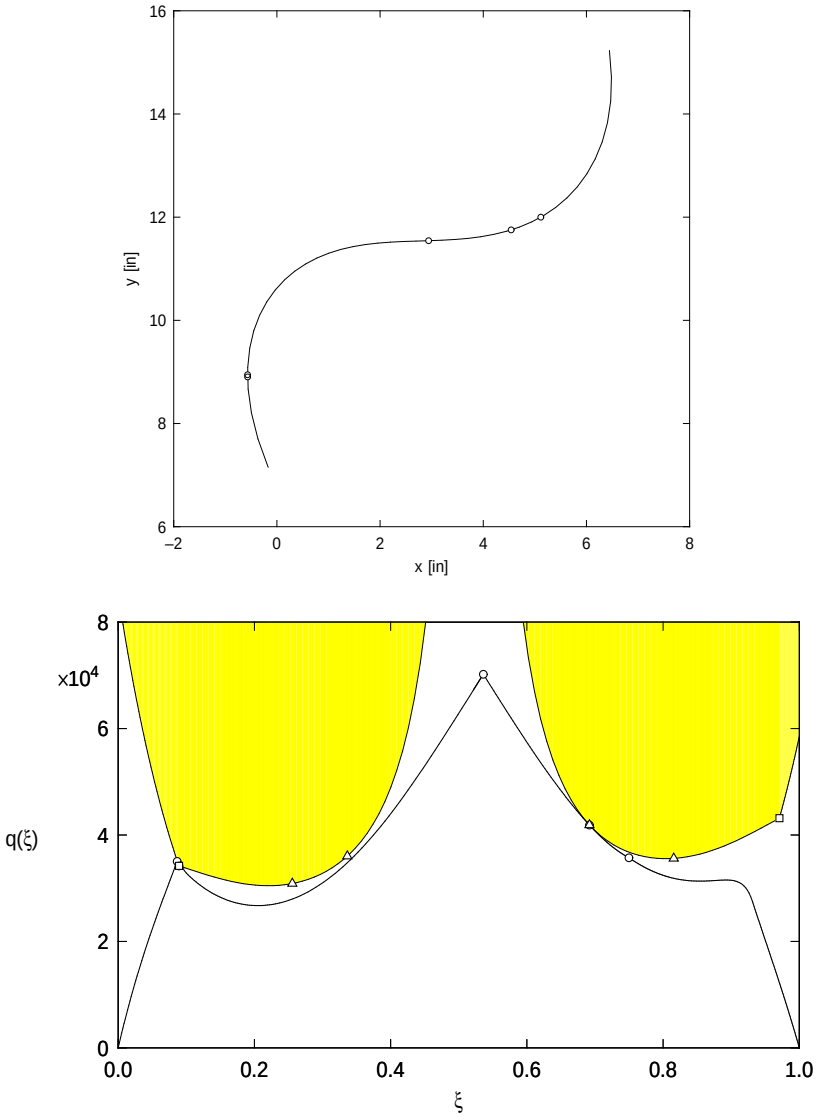

Figure 9: Test curve $\mathbf{r}(\xi)$ (upper) and optimal squared feedrate $q(\xi)$ (lower), with switching points shown. In this case $q(\xi)$ is a piecewise–rational function with two switching points on the velocity limit curve, and three switching points below it (circles indicate switching points below the VLC; squares are critical points on the VLC, and triangles are tangency points on the VLC).

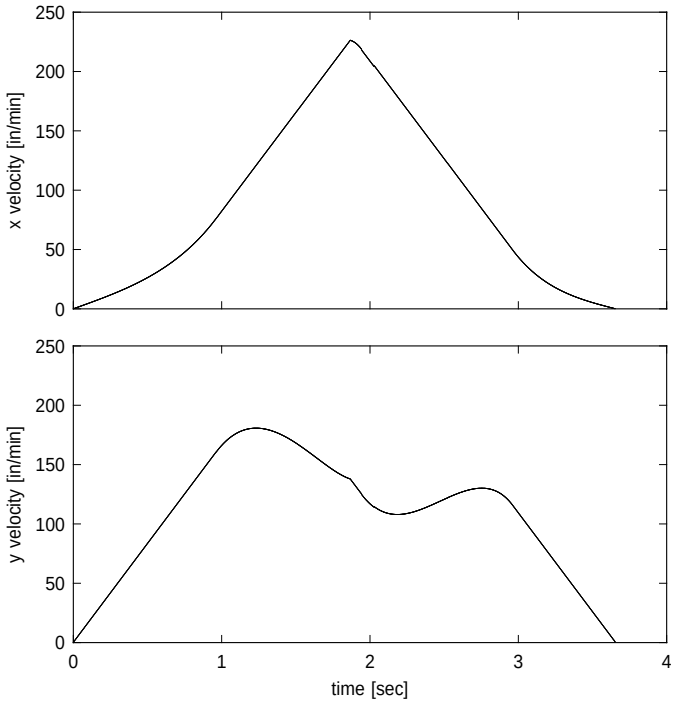

Figure 10: Components of time–optimal feedrate along x and y axes for the curve in Figure 8, obtained from first differences of measured position data.

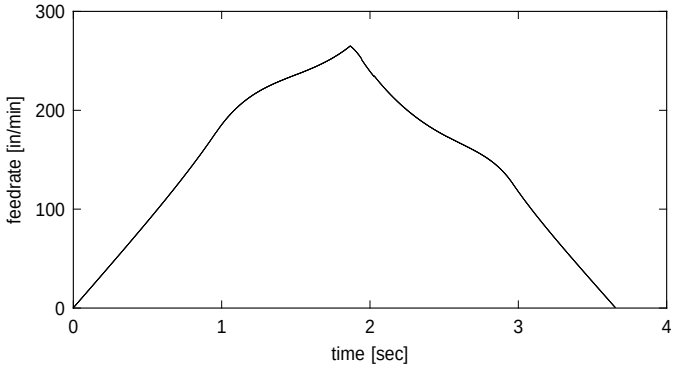

Figure 11: Measured magnitude of time–optimal feedrate v along the curve in Figure 8, obtained from the x and y components illustrated in Figure 10.

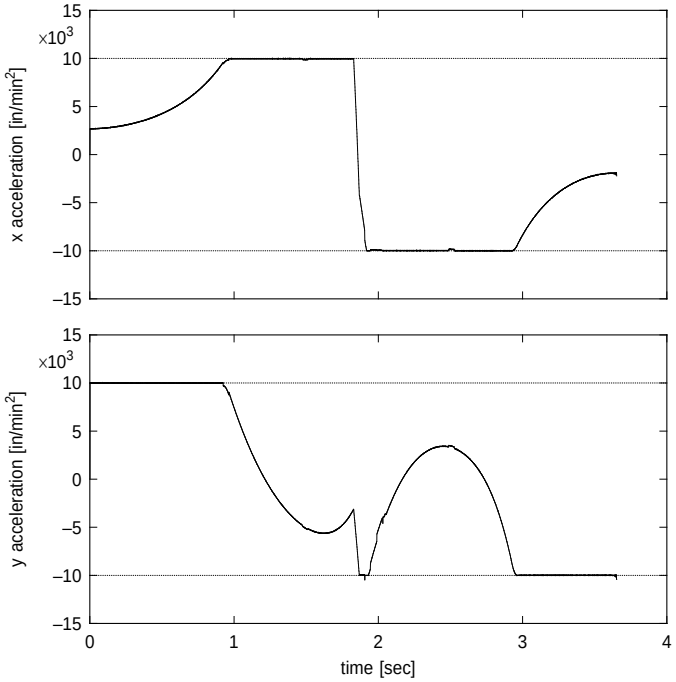

Figure 12: Components of the acceleration along the x and y axes for the test curve in Figure 8, obtained from second differences of the measured position data. Observe that, during each phase of the traversal, either the x or the y acceleration attains the prescribed bounds of $\pm 10^4$ in/min^2.

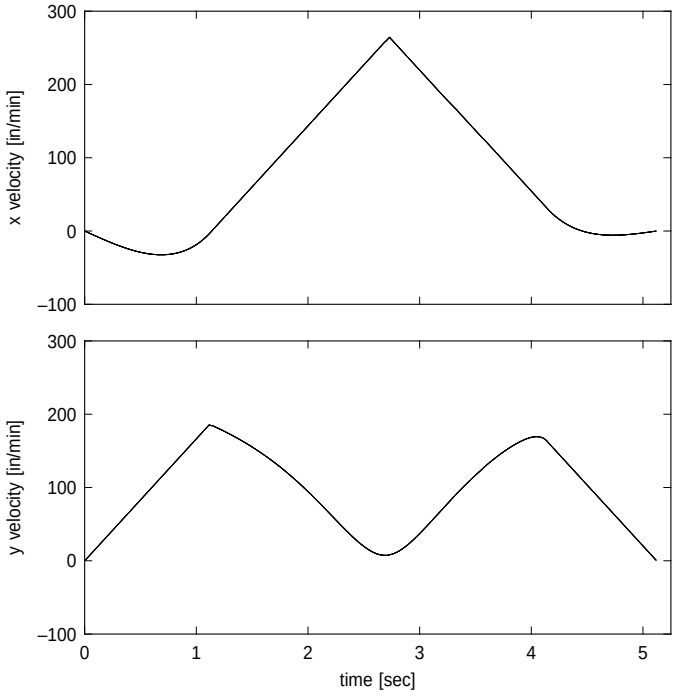

Figure 13: Components of time–optimal feedrate along x and y axes for the curve in Figure 9, obtained from first differences of measured position data.

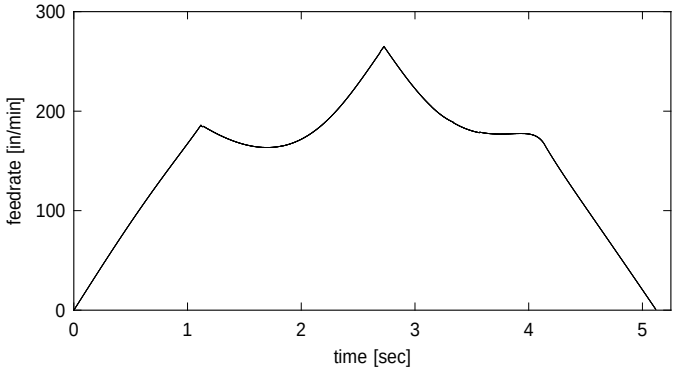

Figure 14: Measured magnitude of time–optimal feedrate v along the curve in Figure 9, obtained from the x and y components illustrated in Figure 13.

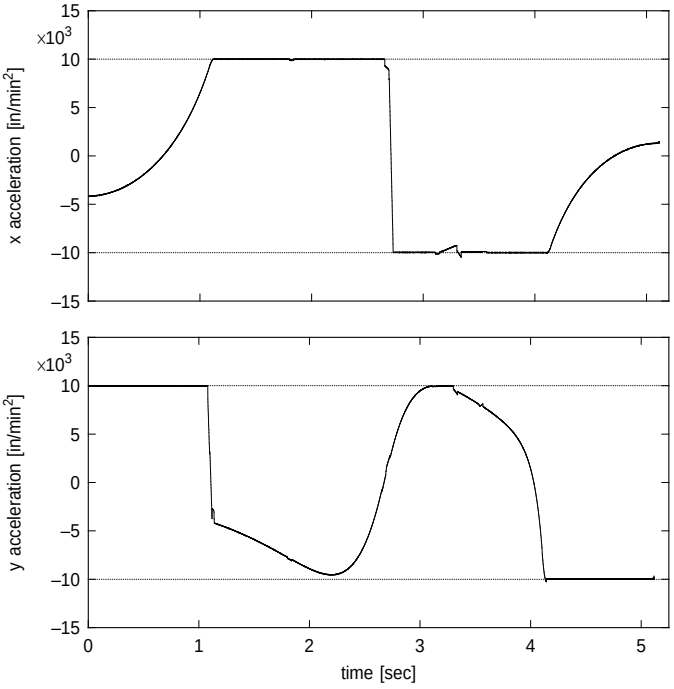

Figure 15: Components of the acceleration along the x and y axes for the test curve in Figure 9, obtained from second differences of the measured position data. Note that, during each of the 6 phases of the traversal, either the x or the y acceleration attains the prescribed bounds of $\pm 10^4$ in/min^2.

10 Closure

The principles of time–optimal motion control subject to prescribed bounds on acceleration, developed [2, 19, 21, 24] in the context of robot manipulator motion, have been applied to the problem of specifying feedrates along curved tool paths in three–axis machining. This context is attractive since, for paths described by polynomial parametric curves, the optimal feedrate admits an exact specification in terms of a piecewise–rational function of the parameter. Furthermore, this feedrate may be realized by a simple real–time interpolator algorithm that drives the machine directly from the analytic path description, eliminating the need for piecewise–linear/circular G code approximations.

In practice, the acceleration bounds should be chosen conservatively based on the known (peak or continuous) motor torque capacity, and the effective inertia of each axis. Since the "ideal" time–optimal feedrate function incurs instantaneous changes in motor torque, it may be desirable to subject the optimal feedrate function $q(\xi)$ to a "smoothing" process, that blends together its rational subsegments in a C^1 or C^2 manner, as a post–processing step. One possible approach is to invoke the Bernstein approximation method [5], using uniformly–sampled values from the optimal feedrate as coefficients. This furnishes a uniformly–convergent "one–sided" C^∞ approximation — one can be certain that the acceleration constraints are never violated, and by increasing the degree of the polynomial the approximation error can be subdued below any prescribed tolerance.

Acknowledgment

This work was supported in part by the National Science Foundation under grant CCR–9902669.

References

[1] EIA Standard RS–274–D (1979), Interchangeable variable block data format for positioning, contouring, and contouring/positioning numerically controlled machines, Electronic Industries Association, Engineering Dept., Washington, D.C.

[2] J. E. Bobrow, S. Dubowsky, and J. S. Gibson (1985), Time–optimal control of robotic manipulators along specified paths, *International Journal of Robotics Research* **4** (3), 3–17.

[3] J.–J. Chou and D. C. H. Yang (1991), Command generation for three–axis CNC machining, *ASME Journal of Engineering for Industry* **113** (August), 305–310.

[4] J.–J. Chou and D. C. H. Yang (1992), On the generation of coordinated motion of five–axis CNC/CMM machines, *ASME Journal of Engineering for Industry* **114** (February), 15–22.

[5] P. J. Davis (1975), *Interpolation and Approximation*, Dover (reprint), New York.

[6] G. Farin (1997), *Curves and Surfaces for Computer Aided Geometric Design* (4th Edition), Academic Press, San Diego.

[7] R. T. Farouki, J. Manjunathaiah, D. Nicholas, G.–F. Yuan, and S. Jee (1998), Variable feedrate CNC interpolators for constant material removal rates along Pythagorean–hodograph curves, *Computer Aided Design* **30**, 631–640.

[8] R. T. Farouki, J. Manjunathaiah, and G.–F. Yuan (1999), G codes for the specification of Pythagorean–hodograph tool paths and associated feedrate functions on open–architecture CNC machines, *International Journal of Machine Tools and Manufacture* **39**, 123–142.

[9] R. T. Farouki and V. T. Rajan (1987), On the numerical condition of polynomials in Bernstein form, *Computer Aided Geometric Design* **4**, 191–216.

[10] R. T. Farouki and V. T. Rajan (1988), Algorithms for polynomials in Bernstein form, *Computer Aided Geometric Design* **5**, 1–26.

[11] R. T. Farouki and T. Sakkalis (1991), Real rational curves are not "unit speed," *Computer Aided Geometric Design* **8**, 151–157.

[12] R. T. Farouki and S. Shah (1996), Real–time CNC interpolators for Pythagorean–hodograph curves, *Computer Aided Geometric Design* **13**, 583–600.

[13] R. T. Farouki and Y–F. Tsai (2001), Exact Taylor series coefficients for variable–feedrate CNC curve interpolators, *Computer Aided Design* **33**, 155–165.

[14] H. Halkin (1965), A generalization of LaSalle's "bang–bang" principle, *SIAM Journal on Control* **2**, 199–202.

[15] J.–T. Huang and D. C. H. Yang (1992), A generalized interpolator for command generation of parametric curves in computer–controlled machines, Proceedings, *Japan/USA Symposium on Flexible Automation*, Vol. 1, ASME, 393–399.

[16] R. Komanduri, K. Subramanian, and B. F. von Turkovich (eds.) (1984), *High Speed Machining*, PED–Vol. 12, ASME, New York.

[17] J. P. LaSalle (1960), The time optimal control problem, in *Contributions to the Theory of Nonlinear Oscillations* (L. Cesari, J. P. LaSalle, and S. Lefschetz, eds.), Vol. 5, Princeton Univ. Press.

[18] R–S. Lin and Y. Koren (1996), Real–time interpolators for multi–axis CNC machine tools, *Manufacturing Systems* **25**, 145–149.

[19] F. Pfeiffer and R. Johanni (1987), A concept for manipulator trajectory planning, *IEEE Journal of Robotics and Automation* **RA–3** (2), 115–123.

[20] Z. Shiller (1994), On singular time–optimal control along specified paths, *IEEE Transactions on Robotics and Automation* **10** 561–566.

[21] Z. Shiller and H. H. Lu (1990), Robust computation of path constrained time optimal motions, Proceedings, *IEEE International Conference on Robotics and Automation*, Cincinnati, OH, 144–149.

[22] Z. Shiller and H. H. Lu (1992), Computation of path constrained time optimal motions with dynamic singularities, *Journal of Dynamic Systems, Measurement, and Control* **114** (March), 34–40.

[23] A. Shima, T. Sasaki, T. Ohtsuki, and Y. Wakinotani (1996), 64–bit RISC–based Series 15 NURBS interpolation, *FANUC Technical Review* **9** (1), 23–28.

[24] K. G. Shin and N. D. McKay (1985), Minimum–time control of robotic manipulators with geometric path contraints, *IEEE Transactions on Automatic Control* **AC-30** (6), 531–541.

[25] M. Shpitalni, Y. Koren, and C. C. Lo (1994), Realtime curve interpolators, *Computer Aided Design* **26**, 832–838.

[26] J. J. E. Slotine and H. S. Yang (1989), Improving the efficiency of time–optimal path–following algorithms, *IEEE Transaction on Robotics and Automation* **5** (1), 118–124.

[27] D. R. Smith (1974), *Variational Methods in Optimization*, Dover (reprint), New York.

[28] S. Smith and J. Tlusty (1997), Current trends in high–speed machining, *ASME Journal of Manufacturing Science and Engineering* **119**, 664–666.

[29] J. Tlusty (1993), High–speed machining, *CIRP Annals* **42**, 733–738.

[30] Y–F. Tsai, R. T. Farouki, and B. Feldman (2001), Performance analysis of CNC interpolators for time–dependent feedrates along PH curves, *Computer Aided Geometric Design* **18**, 245–265.

[31] D. C. H. Yang and T. Kong (1994), Parametric interpolator versus linear interpolator for precision CNC machining, *Computer Aided Design* **26**, 225–234.

[32] H. S. Yang and J. J. E. Slotine (1994), Fast algorithms for near–minimum–time control of robot manipulators, *International Journal of Robotics Research* **13**, 521–532.

[33] S–S. Yeh and P–L. Hsu (1999), The speed–controlled interpolator for machining parametric curves, *Computer Aided Design* **31**, 349–357.